Preprints.org

Article

Not peer-reviewed version

Visualization of Lubrication Conditions Using the Electrical Impedance Method Considering Surface Roughness

Daichi Kosugi , Fumiaki Aikawa , Shunsuke Iwase , Taisuke Maruyama * , Satoshi Momozono

Posted Date: 4 March 2026

doi: 10.20944/preprints202603.0309.v1

Keywords: electrical impedance method; condition monitoring; oil film thickness; surface roughness; electric field analysis; elastohydrodynamic lubrication

Preprints.org is a free multidisciplinary platform providing preprint service that is dedicated to making early versions of research outputs permanently available and citable. Preprints posted at Preprints.org appear in Web of Science, Crossref, Google Scholar, Scilit, Europe PMC.

Copyright: This open access article is published under a Creative Commons CC BY 4.0 license, which permit the free download, distribution, and reuse, provided that the author and preprint are cited in any reuse.

Preprints.org (www.preprints.org) | NOT PEER-REVIEWED | Posted: 4 March 2026 doi:10.20944/preprints202603.0309.v1

Disclaimer/Publisher's Note: The statements, opinions, and data contained in all publications are solely those of the individual author(s) and contributor(s) and not of MDPI and/or the editor(s). MDPI and/or the editor(s) disclaim responsibility for any injury to people or property resulting from any ideas, methods, instructions, or products referred to in the content.

Article

Visualization of Lubrication Conditions Using the Electrical Impedance Method Considering Surface Roughness

Daichi Kosugi [1], Fumiaki Aikawa [1,2], Shunsuke Iwase [1], Taisuke Maruyama [1,*] and Satoshi Momozono [2]

[1] NSK Ltd., 1-5-50 Kugenuma-shinmei, Fujisawa 251-8501, Japan

[2] Institute of Science Tokyo, 4259, Nagatsuta, Midori Yokohama 226-8501, Japan

* Correspondence: maruyama-ta@nsk.com

Abstract

In this study, we developed an improved electrical impedance method for measuring oil film thickness with a correction for surface roughness effects. Statistical analysis of the oil film thickness distribution revealed that rough surfaces exhibit higher capacitance values than those predicted by the ideal parallel-plate model, despite having the same mean film thickness. Consequently, a corresponding roughness correction formula was derived. The accuracy of the method was verified in ball-on-disc type apparatus using balls with a rough surface. The corrected oil film thickness agreed more closely with the Hamrock-Dowson equation and with optical interferometry measurements than did the uncorrected result. These outcomes confirm that oil film thickness can be estimated considering surface roughness. The technique is therefore expected to facilitate the optimization of lubrication conditions and enable more reliable bearing-life prediction.

Keywords: electrical impedance method; condition monitoring; oil film thickness; surface roughness; electric field analysis; elastohydrodynamic lubrication

1. Introduction

Rolling bearings are widely utilized as key components to effectively support rotating parts in various mechanical devices. When lubricants such as oil or grease are supplied, extremely thin oil films form between the surfaces. Under these conditions, elastohydrodynamic (EHD) lubrication occurs, which reduces friction and wear by preventing direct metallic contact [1]. This mechanism enables bearings to achieve smooth and stable rotational operation even under high load conditions. The Hamrock-Dowson equation has been established as the standard prediction model for EHD film thickness and is widely used for evaluating oil film thickness in rolling bearings under fully flooded lubrication [2].

For stable low-torque operation of rolling bearings, monitoring technology is essential for accurately capturing operating conditions and for maintaining optimal oil film thickness. While condition monitoring methods are diverse, vibration analysis is the most widely used technique, and its effectiveness has been demonstrated in numerous experiments. When damage occurs on metal surfaces and track surface smoothness is compromised, vibration magnitude increases rapidly. Furthermore, since inner rings, outer rings, and rolling elements each have characteristic passing frequencies, it has been reported that damage locations can be identified through frequency analysis [3–6]. Research has also been conducted on acoustic emission, which is elastic waves released during material damage [7]. However, these monitoring methods can only detect damage after it has progressed enough for significant signals to be generated, limiting their capability for failure prediction and immediate optimization of operating conditions.

© 2026 by the author(s). Distributed under a Creative Commons CC BY license.

Preprints.org (www.preprints.org) | NOT PEER-REVIEWED | Posted: 4 March 2026 doi:10.20944/preprints202603.0309.v1

Meanwhile, approaches for measuring oil film thickness in the EHD contact area have attracted attention, with fundamental tests using optical interferometry being conducted [8–11]. However, these require transparent materials and are difficult to apply to metallic rolling bearings. Therefore, electrical methods have been proposed. The contact-resistance method applies a small DC voltage across the two surfaces; when the oil film collapses and metallic contact forms, the circuit closes and a sharp decrease in resistance is detected. This change in DC resistance serves as an indicator of oil film breakdown and has been shown to correlate strongly with film thickness and other lubrication parameters [12,13]. Additionally, capacitance methods, which treat the EHD contact area as capacitors, have demonstrated the ability to quantify oil film thickness in both fundamental testing and actual bearing testing [14–17]. More recently, Maruyama and Nakano proposed the electrical impedance method (EIM) [18]. The EIM applies an AC voltage to the contact area and simultaneously estimates thickness and breakdown ratio of oil films from the resulting complex impedance. Therefore, it is superior to conventional capacitance-based and DC contact-resistance methods. Oil film thickness obtained by EIM for single EHD contact agrees well with optical measurement results and the Hamrock-Dowson equation, and applicability to deep groove ball bearings and to needle roller bearings with line contact has also been confirmed [19,20]. Furthermore, Iwase et al. demonstrated that oxidative degradation of lubricants can be detected from dielectric properties obtained by sweeping the applied frequency [21], and Maruyama et al. showed the possibility of in-situ wear measurement from abnormal increases in dielectric constant in steel–steel contacts [22]. Additionally, monitoring of lubrication conditions through EIM application to gears, which similarly have sliding components, has been actively conducted [23,24].

However, current EIM models approximate the contact area separated by an oil film as a parallel-plate capacitor and compute mean film thickness from the capacitance. Consequently, they fail to capture the real film thickness distribution and the influence of surface roughness. Given the well-established effect of surface roughness on capacitance, various analytical approaches explicitly incorporating this factor have been widely employed in electronics and materials science [25–27]. However, because these analyses assume an electrode separation distance is much larger than the characteristic surface roughness, they have not yet been applied at the scale of the EHD contact area. In EHD contacts, the oil film thickness is typically on the order of tens to hundreds of nanometers, which is comparable to the surface roughness amplitude. Therefore, the assumption of large electrode separation relative to roughness does not hold in this regime. Surface roughness in the tribology field has been evaluated from multiple perspectives, including statistical contact analysis [28], prediction of peak density and curvature using Power Spectral Density [29], and consideration of surface roughness in Reynolds equations [30], as they affect friction and wear characteristics as well as fluid flow. Electrical approaches have also been explored in tribology: Morris et al. analyzed electric field strength in rough EHD conjunctions [31], and Sunahara et al. developed a device for observing grease film breakdown through electrical measurement [32]. Furthermore, electrochemical impedance spectroscopy has been applied to evaluate surface roughness and morphology [33]. However, none of these studies directly addressed how surface roughness alters capacitance in the EHD contact area.

Therefore, this study introduces surface roughness concepts into EIM and theoretically analyzes the effects of oil film thickness distribution on complex impedance. Specifically, by constructing a modified capacitance model incorporating statistical roughness parameters and incorporating it as a correction term into conventional models, an improvement in oil film thickness estimation accuracy was proposed. This paper reports on the theoretical framework and verification results through fundamental experiments.

2. Measurement Principle

In the EIM, the EHD contact area S is represented by an RC parallel circuit. The resistive branch stands for metallic contact, and the capacitive branch stands for the lubricant film. Fitting the measured complex impedance Z to this circuit gives the breakdown ratio of oil films α and the mean film thickness h_1. In the conventional approximation, the capacitive branch is treated as a parallel-

© 2026 by the author(s). Distributed under a Creative Commons CC BY license.

Preprints.org (www.preprints.org) | NOT PEER-REVIEWED | Posted: 4 March 2026 doi:10.20944/preprints202603.0309.v1

plate capacitor. The capacitance C_1 is then estimated by regarding whole contacts as two flat electrodes separated by a uniform gap $h_{1,\mathrm{flat}}$,

$$C_1 = \varepsilon_0 \varepsilon_r \frac{(1-\alpha)S}{h_{1,\mathrm{flat}}} = \varepsilon \frac{(1-\alpha)S}{h_{1,\mathrm{flat}}} \tag{1}$$

where ε is the permittivity of the lubricant.

The conventional circuit also places the capacitance C_2 of the region that surrounds the contact in parallel with C_1. Using the measured impedance magnitude $|Z|$ and phase angle θ at each angular frequency ω, the model calculates the mean film thickness $h_{1,\mathrm{flat}}$. Given that r_b is the ball radius and c is the Hertzian contact radius, the film thickness predicted by the electrical impedance method, $h_{1,\mathrm{flat}}$ is then

$$h_{1,\mathrm{flat}} = \frac{(1-\alpha)c^2}{2r_\mathrm{b}} / \mathfrak{W}\left(\frac{(1-\alpha)c^2}{2{r_\mathrm{b}}^2}\exp\left(1 - \frac{\sin\theta}{2\pi\varepsilon\omega r_\mathrm{b}|Z|}\right)\right) \tag{2}$$

where $\mathfrak{W}$ denotes the Lambert W function. Let $\bar{h}_{\mathrm{flat}}$ be the mean oil film thickness over the entire contact area S; then the following relation holds.

$$\bar{h}_{\mathrm{flat}} = (1-\alpha)h_{1,\mathrm{flat}} \tag{3}$$

In practice, surface roughness causes the local film thickness to vary spatially, reflecting the underlying surface height distribution. The lubricant film at any point on the contact (x, y) can therefore be written as $h(x, y)$. This non-uniform film induces a three-dimensional electric field distribution $E(x, y, z)$; field crowding near asperity summits, for example, can raise the apparent capacitance. To treat this rigorously, the local electrostatic energy density u is introduced,

$$u(x,y,z) = \frac{1}{2}\varepsilon E(x,y,z)^2 \tag{4}$$

and evaluate the total electrostatic energy U.

$$U = \iiint_V u(x,y,z)\,\mathrm{d}x\mathrm{d}y\mathrm{d}z \tag{5}$$

The capacitance C and the stored energy are related by the following equation:

$$C = \frac{2U}{V^2} \tag{6}$$

where V is the applied voltage. Thus, when the opposing surfaces are rough, the capacitance C must be obtained by integrating the spatially varying energy density u over every volume element in the gap. As a practical way to treat the electric-field distribution, the rough surface capacitor is approximated as an array of discrete parallel-plate capacitors connected in parallel. Under this approximation, once the coordinates x and y are fixed, the electrostatic-energy density is constant with respect to z. The following relation is obtained:

$$u(x,y) = \frac{1}{2}\varepsilon E(x,y)^2 = \frac{\varepsilon V^2}{2h(x,y)^2} \tag{7}$$

$$U = \iint u(x,y)h(x,y)dxdy \tag{8}$$

$$C_1 = \varepsilon \iint \frac{dxdy}{h(x,y)} \tag{9}$$

Let H be a random variable representing the film thickness, with probability density function $f(h)$, so that

$$C_1 = \int_{h_{\min}}^{h_{\max}} \varepsilon \frac{(1-\alpha)S}{h} f(h)\,\mathrm{d}h = \varepsilon(1-\alpha)S\mathbb{E}\left[\frac{1}{H}\right] \tag{10}$$

© 2026 by the author(s). Distributed under a Creative Commons CC BY license.

Preprints.org (www.preprints.org) | NOT PEER-REVIEWED | Posted: 4 March 2026 doi:10.20944/preprints202603.0309.v1

where $\mathbb{E}[\cdot]$ is the expectation operator. Given that the capacitance C is obtained experimentally, Equations (1) and (10) lead to the following relation.

$$\frac{1}{h_{1,\mathrm{flat}}} = \mathbb{E}\left[\frac{1}{H}\right] \tag{11}$$

Because the function

$$g(x) = \frac{1}{x} \tag{12}$$

is convex on the positive real line, Jensen's inequality applies,

$$g(\mathbb{E}[H]) \leq \mathbb{E}[g(H)] \tag{13}$$

These results indicate that the predicted capacitance considering surface roughness is consistently greater than that predicted by the ideal parallel-plate model [34].

Under fully flooded lubrication, the minimum film thickness $h_{\min}$ remains positive and poses no difficulty. However, once metallic contact occurs, certain points on the real surface profile have zero gap, causing the capacitance integral to diverge. To circumvent this problem, metallic contact areas are excluded and only regions that retain a lubricant film thick enough to act as a capacitor are considered. In addition, when the local electric field exceeds the dielectric breakdown strength E_b of the oil, the lubricant no longer behaves as a dielectric. Regions in which the field surpasses E_b are therefore likewise omitted. With these constraints, $h_{\min}$ can be treated as positive.

To evaluate $\mathbb{E}[1/H]$, the film thickness distribution represented by the random variable H is described by an appropriate probability density function. Although surface roughness on engineering components is often well approximated by a normal distribution, this choice is inconvenient here because its domain includes zero, which makes $\mathbb{E}[1/H]$ undefined. A truncated normal distribution with domain (> 0) avoids this singularity yet yields no explicit elementary expression for $\mathbb{E}[1/H]$. A more practical choice is the gamma distribution, whose shape can approximate a normal distribution for appropriate parameters and whose support is strictly positive. As Greenwood and Williamson examined the exponential distribution as an alternative to the normal [28], it can be considered reasonable to employ the gamma distribution, which generalizes the exponential distribution, for the similar purpose. When the film thickness H is assumed to follow a gamma distribution with shape parameter a and rate parameter b, the probability density function is

$$H \sim \mathrm{Ga}(a,b), \qquad f\,(h \mid a,b) = \frac{b^a}{\Gamma(a)} h^{a-1}\exp(-bh)\,, h > 0 \tag{14}$$

where $\Gamma(\cdot)$ denotes the gamma function. The gamma parameters a and b can be obtained from the mean film thickness considering roughness $h_{1,\mathrm{rough}}$ and the standard deviation of the film thickness distribution σ by the method of moments:

$$a = \left(\frac{h_{1,\mathrm{rough}}}{\sigma}\right)^2, \qquad b = \frac{h_{1,\mathrm{rough}}}{\sigma^2} \tag{15}$$

Unlike the normal or truncated-normal distributions, the gamma distribution allows a simple closed-form expression for the E $[1/H]$. For a gamma-distributed film thickness, $\mathbb{E}[1/H]$ is

$$\mathbb{E}\left[\frac{1}{H}\right] = \int_0^\infty \frac{1}{h}\frac{b^a}{\Gamma(a)} h^{a-1}\exp(-bh)dh = \frac{b^a}{\Gamma(a)}\int_0^\infty h^{a-2}\exp(-bh)dh \tag{16}$$

The condition $a > 1$ is necessary because the integral in Eq. (16) diverges when $a \leq 1$, corresponding to $\Gamma(a-1)$ being undefined. By employing the gamma function relation in Eq. (17) gives a compact expression for $\mathbb{E}[1/H]$ in terms of the shape and rate parameters a and b:

$$\int_0^\infty h^{a-2}\exp(-bh)dh = \frac{\Gamma(a-1)}{b^{a-1}} \tag{17}$$

© 2026 by the author(s). Distributed under a Creative Commons CC BY license.

Preprints.org (www.preprints.org) | NOT PEER-REVIEWED | Posted: 4 March 2026 doi:10.20944/preprints202603.0309.v1

$$\mathbb{E}\left[\frac{1}{H}\right] = \frac{b^a \Gamma(a-1)}{b^{a-1}\Gamma(a)} = \frac{b}{a-1} \quad (a > 1) \tag{18}$$

Thus, using equation (15), $\mathbb{E}[1/H]$ can be expressed solely in terms of the $h_{1,\mathrm{rough}}$ and the σ.

$$\mathbb{E}\left[\frac{1}{H}\right] = \frac{h_{1,\mathrm{rough}}}{{h_{1,\mathrm{rough}}}^2 - \sigma^2} \tag{19}$$

Substituting this relation into Eq. (11), yields a quadratic equation in $h_{1,\mathrm{rough}}$, retaining the positive root expresses $h_{1,\mathrm{rough}}$ explicitly as a function of $h_{1,\mathrm{flat}}$.

$${h_{1,\mathrm{rough}}}^2 - h_{1,\mathrm{flat}} h_{1,\mathrm{rough}} - \sigma^2 = 0 \tag{20}$$

$$h_{1,\mathrm{rough}} = \frac{h_{1,\mathrm{flat}}}{2}\left(1 + \sqrt{1 + \left(\frac{2\sigma}{h_{1,\mathrm{flat}}}\right)^2}\right) \tag{21}$$

When the metallic contact region is included, the overall mean film thickness $\bar{h}_{\mathrm{rough}}$ can be written in the same form as Eq. (3):

$$\bar{h}_{\mathrm{rough}} = (1-\alpha) h_{1,\mathrm{rough}} \tag{22}$$

By applying this equation, the conventional value $\bar{h}_{\mathrm{flat}}$ can be corrected using the σ to obtain the roughness adjusted mean film thickness $\bar{h}_{\mathrm{rough}}$.

3. Experimental Details

3.1. Measurement Apparatus

Figure 1 shows the ball-on-disc type apparatus used in this study. A steel ball with a radius of 12.7 mm rolls against a BK7 glass disc (diameter 100 mm, thickness 10 mm). The disc was coated with a 5 nm semi-reflective chromium film, followed by an electrically conductive 1 μm ITO spacer layer. The ball is fixed to a horizontal shaft driven by a servo motor, and the disc is mounted on a vertical shaft driven by another motor. The two spindles are synchronized so that their circumferential speed v is the same, 0.05 m/s to 0.50 m/s, which sets the slip ratio to zero. The lower hemisphere of the ball dips into the oil bath and entrains lubricant into the contact. White light from a microscope illuminates the contact (see Figure 2). Part of the beam is reflected at the chromium layer; the remainder passes through the ITO spacer and oil film, then reflects at the ball surface. A beam-splitter divides the interfered light. One branch is recorded directly by a high-speed camera to visualize the lubricant condition, while the other is directed through a slit within the spectrometer to a second camera that provides quantitative film thickness measurements. Since rough ball surfaces scatter light diffusely, optical interferometry was performed only on the smooth ball. An LCR meter applies a sinusoidal voltage of 0.2 V rms at 100 kHz across the contact. The resulting current is measured to obtain the complex impedance Z. Slip rings on each shaft maintain electrical connection, and rubber couplings insulate the disc from the rest of the shaft. Post-processing of Z yields the oil film thickness without considering surface roughness $\bar{h}_{\mathrm{flat}}$ and the breakdown ratio α. A torque sensor on the vertical spindle records the torque required to rotate the disc under a load of F_N = 22.4 N. The friction coefficient μ is expressed in terms of the measured torque M, the track radius R_t, and the applied load F_N as follows

$$\mu = \frac{M}{R_t F_N} \tag{23}$$

© 2026 by the author(s). Distributed under a Creative Commons CC BY license.

Preprints.org (www.preprints.org) | NOT PEER-REVIEWED | Posted: 4 March 2026 doi:10.20944/preprints202603.0309.v1

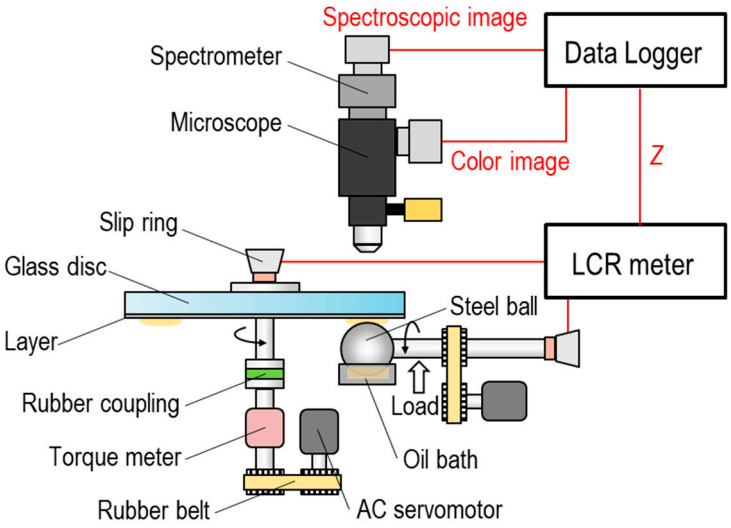

Figure 1. Schematic diagram of the ball-on-disc apparatus equipped with optical interferometry.

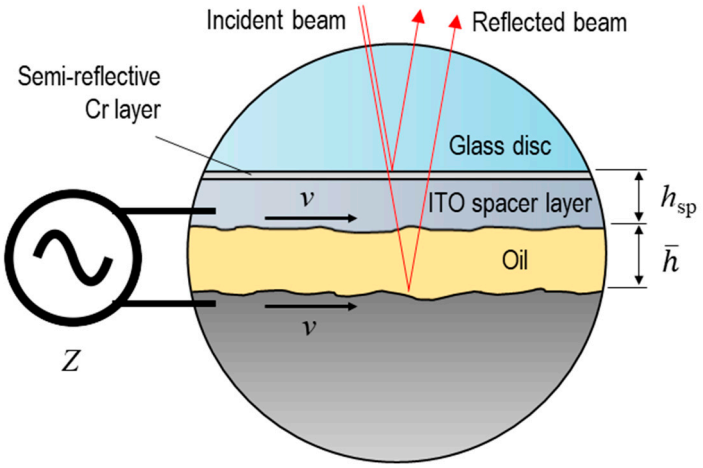

Figure 2. Schematic diagram of simultaneous film thickness measurement by optical interferometry and EIM.

3.2. Materials

The ball specimen is made of AISI 52,100 steel with a Young's modulus of 208 GPa and a Poisson's ratio of 0.30. The disc specimen is fabricated from BK7 optical glass with a Young's modulus of 72 GPa and a Poisson's ratio of 0.26. Surface measurements were performed using optical interference microscopy. Surface roughness parameters, namely the standard deviation σ, skewness γ_1, and kurtosis γ_2 were calculated from the height distribution after removal of the spherical form but without waviness filtering, and are listed in Table 1 for both specimens. Additionally, corresponding two-dimensional height maps and histograms are provided in Figures 3 and 4. The lubricant is a poly-α-olefin (PAO) base oil. It has a kinematic viscosity of 426.6 mm²/s at 40 °C and a relative permittivity of $\varepsilon_r = 2.1$ at 25 °C and 100 kHz.

Table 1. Surface roughness parameters of test specimens.

Parameter	Disc	Ball 0	Ball 1	Ball 2
σ [nm]	0.89	2.37	382.79	478.44
γ_1 [–]	-0.285	-0.666	-1.218	-0.548
γ_2 [–]	106.5*	4.167	4.844	2.960

*Abnormal kurtosis value affected by pinholes.

© 2026 by the author(s). Distributed under a Creative Commons CC BY license.

Preprints.org (www.preprints.org) | NOT PEER-REVIEWED | Posted: 4 March 2026 doi:10.20944/preprints202603.0309.v1

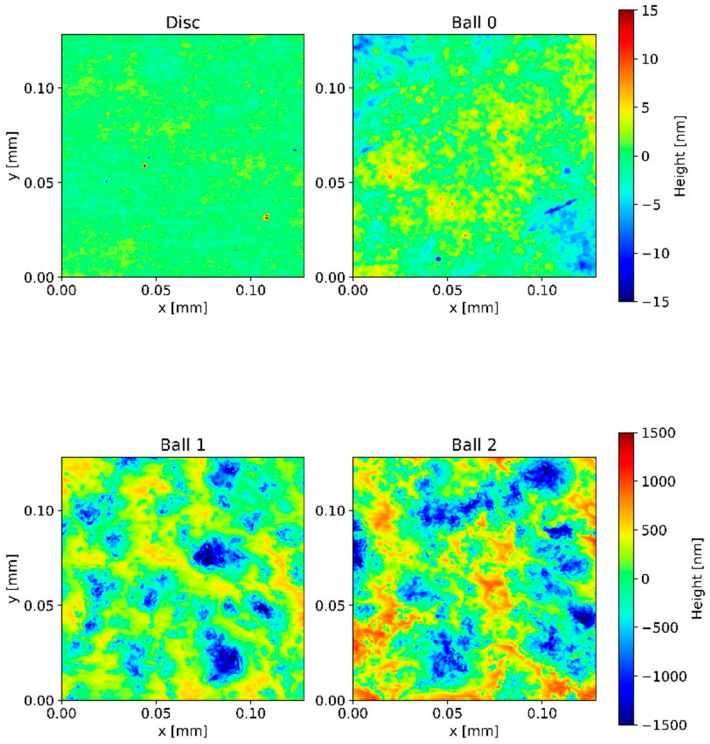

Figure 3. Two-dimensional color maps of the surface height distributions for each specimen.

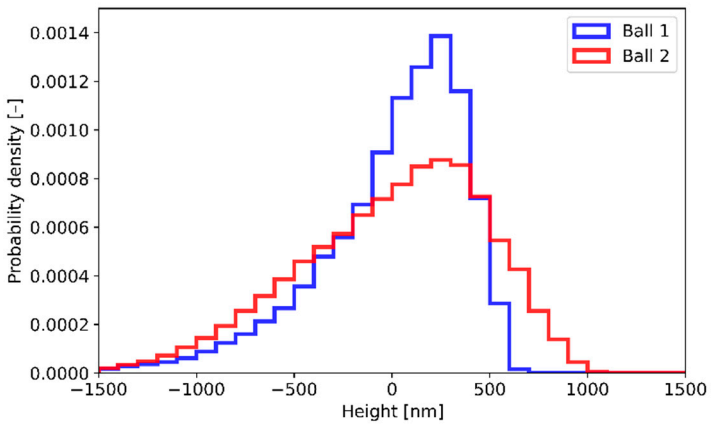

Figure 4. Histogram of the surface-height distributions for Ball 1 (blue) and Ball 2 (red), with each profile shifted so that its mean height is zero.

3.3. Procedure

Prior to testing, the ball, disc, and oil bath were ultrasonically cleaned in hexane, and dried. The components were then assembled, and the bath was filled with PAO. With the ball pressed against the stationary disc, a reference interferogram was captured to determine the spacer-layer thickness, and the static complex impedance was measured. Afterward, the spindles were accelerated to the prescribed speed and the ball was re-loaded against the disc with the specified normal force. For each circumferential-speed condition, film thickness interferograms, electrical impedance data, and friction torque were recorded simultaneously. All experiments were carried out in a laboratory maintained at 25 ± 0.5 °C.

© 2026 by the author(s). Distributed under a Creative Commons CC BY license.

Preprints.org (www.preprints.org) | NOT PEER-REVIEWED | Posted: 4 March 2026 doi:10.20944/preprints202603.0309.v1

4. Experimental Results

The results obtained by applying the proposed equation to the oil film thickness measured in the ball-on-disc tests are shown in Figure 5. For balls with rough surfaces, the $\bar{h}_{\mathrm{flat}}$ values represented by open circles, were lower than the Hamrock-Dowson equation in the v range where the contact ratio α and the friction coefficient μ begin to increase. In contrast, the $\bar{h}_{\mathrm{rough}}$ values represented by filled circles, showed good agreement with the Hamrock-Dowson equation, the central film thickness measured by optical interferometry, and the oil film thickness of Ball 0, which had an extremely smooth surface. This agreement was observed in the speed range above 0.1 m/s, suggesting that the proposed correction successfully compensates for the increase in capacitance caused by surface roughness. In the lower v range, below 0.1 m/s, $\bar{h}_{\mathrm{rough}}$ converged to an approximately constant value, which was nearly equal to σ.

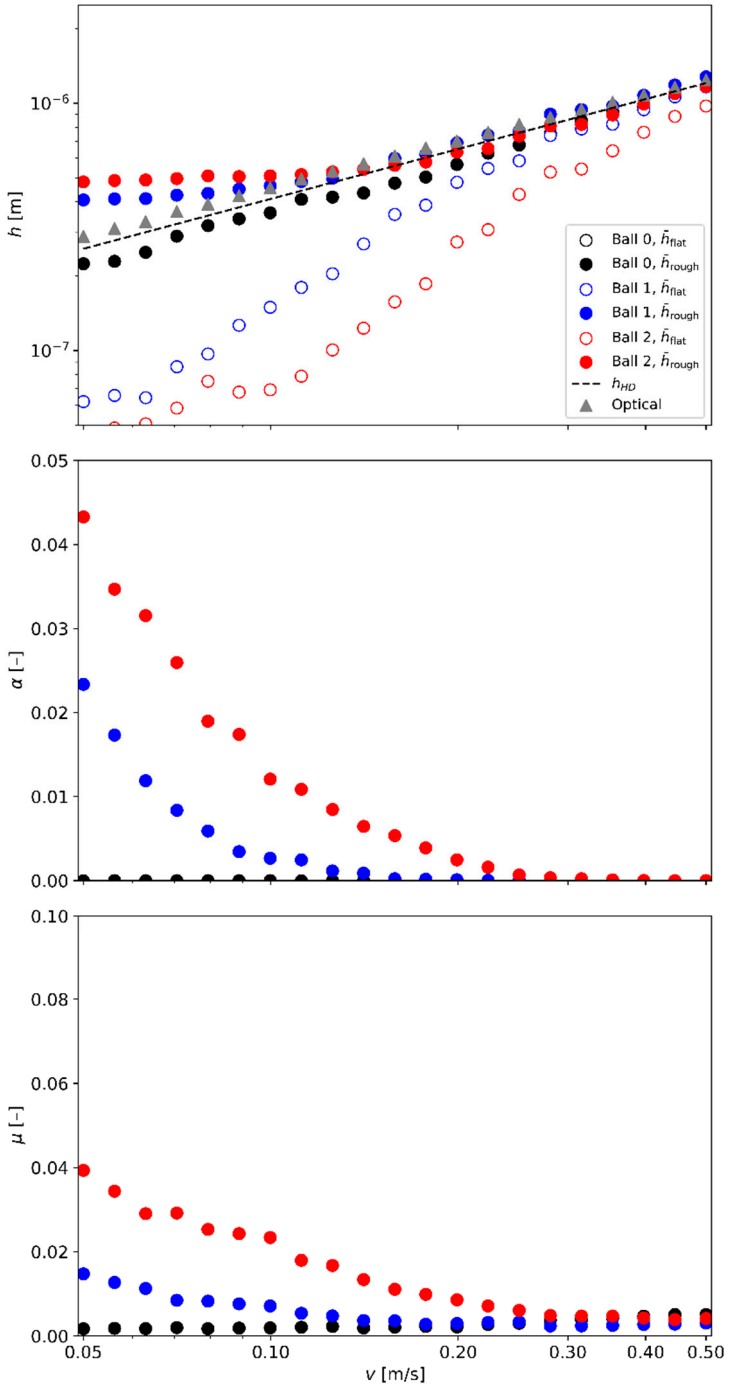

© 2026 by the author(s). Distributed under a Creative Commons CC BY license.

Preprints.org (www.preprints.org) | NOT PEER-REVIEWED | Posted: 4 March 2026 doi:10.20944/preprints202603.0309.v1

Figure 5. Measured values of oil film thickness h (top), breakdown ratio α (middle), and friction coefficient μ (bottom) as a function of entrainment speed v. Lubricant: PAO (kinematic viscosity at 40 °C: 426.6 mm²/s); normal load: F_N = 22.4 N; slide-to-roll ratio: 0 (pure rolling). In the top graph: open circles denote values obtained with the conventional method; filled circles are values corrected for the σ of surface roughness obtained by optical interference microscope; grey triangles indicate the central film thickness measured simultaneously by optical interferometry; the black dashed line represents the Hamrock-Dowson equation.

5. Discussion

5.1. Validity of Assuming Surface Height Distribution as a Parallel-Plate Model

This study assumes that, once the gap distance between infinitesimal surface elements is specified, the electric field remains uniform; in other words, the spatial field distribution is not considered, and the Laplace equation is not solved. To verify the validity of this simplification, we computed the capacitance and compared the results with those obtained from a more rigorous analysis. Surface-profile data for the ball, acquired with an optical interferometer were inverted and offset by a prescribed $\bar{h}$ to generate a two-dimensional array of the film thickness. Because the roughness of the disc is negligibly small relative to that of the ball, σ for the disc surface was set to zero. Cases in which the maximum asperity height exceeded $\bar{h}$, giving non-positive gap values (i.e., solid contact), were excluded. Capacitance for this gap field was evaluated by two methods. The first method employed electrostatic finite-element analysis using COMSOL® Multiphysics (version 6.2). The gap domain was discretized, constant electric potentials were applied to the two bounding surfaces, and the Laplace equation was solved to obtain the potential distribution. The electric field was then derived from the gradient of the potential, and the capacitance was calculated by theoretical procedure. Because interactions between neighboring elements are fully considered, this method yields the most rigorous solution. Figure 6 shows a representative electric field distribution for Ball 1 at $\bar{h}/\sigma$ = 3 and under an applied voltage of 1.0 V.

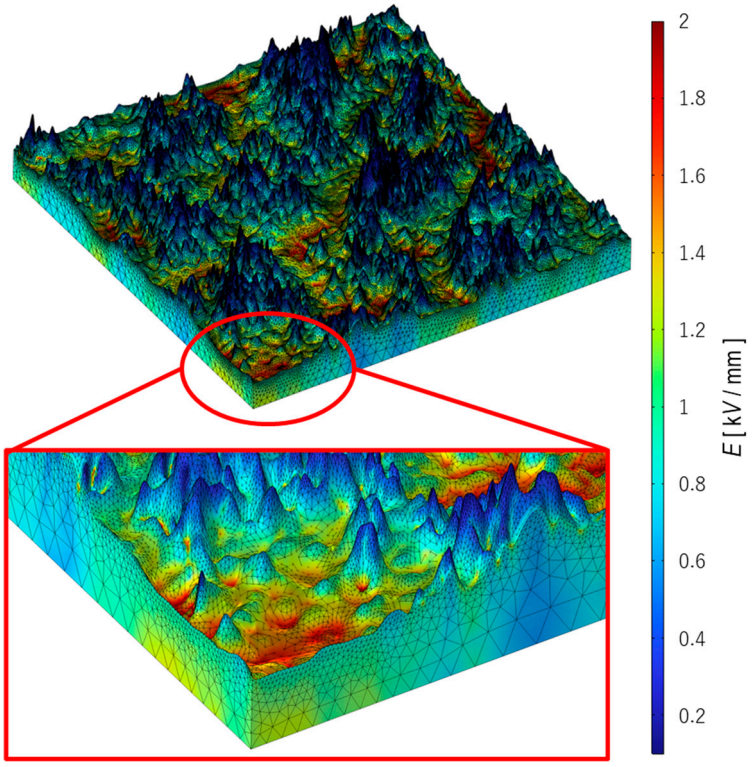

Figure 6. Example of finite-element analysis of the electric field using surface-height data obtained by optical interferometry. The calculation was performed for Ball 1 with $\bar{h}/\sigma$ = 3 under an applied voltage of 1.0 V.

© 2026 by the author(s). Distributed under a Creative Commons CC BY license.

Preprints.org (www.preprints.org) | NOT PEER-REVIEWED | Posted: 4 March 2026 doi:10.20944/preprints202603.0309.v1

The second approach idealizes each pixel of the gap (pixel indices $i, j = 1, \ldots, n$) as an independent parallel-plate capacitor that does not interact electrostatically with its neighbors. The capacitance of every pixel is evaluated individually from its local separation, and the overall capacitance C is approximated by connecting these elemental capacitors in parallel and summing their contributions. Denoting the surface-height distributions of the disc and ball by d_{ij} and b_{ij}, respectively, the local oil film thickness h_{ij} and the total capacitance are expressed as below.

$$h_{ij} = d_{ij} - b_{ij} + \bar{h} \tag{24}$$

$$C = \sum_{i}^{n} \sum_{j}^{n} \varepsilon \frac{S/n^2}{h_{ij}} \tag{25}$$

Although this pixel-based model sacrifices accuracy by neglecting electrostatic coupling between elements, it offers a significant gain in computational efficiency. The capacitances predicted by the electrostatic finite-element analysis and the parallel-plate approximation were compared to validate the simpler model. Figure 7 compares the capacitances obtained with the two numerical schemes. The horizontal axis is the $\bar{h}/\sigma$, which corresponds to the film parameter Λ; the vertical axis is the capacitance normalized by that of an ideal parallel flat capacitor whose gap equals $\bar{h}$. For every film thickness regime the normalized capacitance exceeds unity, indicating that surface roughness always enhances the capacitance relative to the flat-plate configuration. This enhancement becomes markedly larger as the film thickness decreases. The finite-element results (symbols) consistently exceeded those of the parallel-plate model (solid lines). The difference between the two predictions arises because the parallel-plate model does not solve Laplace's equation and therefore cannot capture the mutual electric-field interactions that develop when asperities are very close to each other. This limitation becomes increasingly pronounced for roughness components with high wavenumbers. A detailed discussion of this effect is given in Appendix A. Nevertheless, the two curves lie so close together that, for the surface textures and film thickness range investigated here, treating each pixel as an independent parallel-plate capacitor can reasonably be considered acceptable.

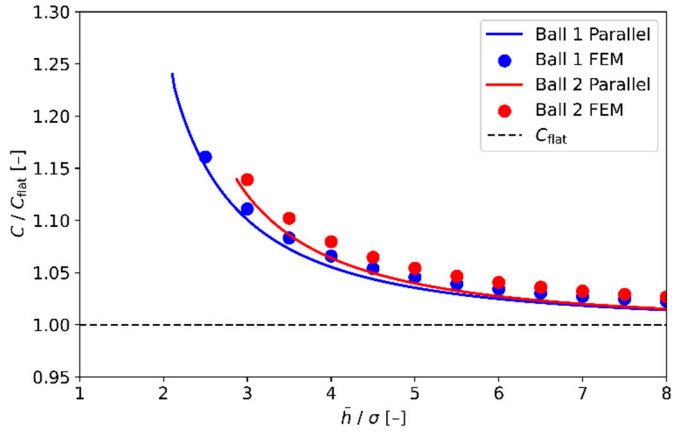

Figure 7. Capacitance ratio C/C_{flat} as a function of the $\bar{h}/\sigma$. Solid curves give the parallel-plate approximation, while circular markers denote electrostatic finite-element results (FEM). Blue symbols/lines correspond to Ball 1 and red to Ball 2. The dashed horizontal line indicates the baseline condition $C = C_{flat}$ (ratio = 1).

5.2. Validity of Assuming Oil Film Thickness Distribution as a Gamma Distribution

The validity of describing the gap-height distribution with a gamma distribution was examined. Figure 8 shows, for each ball, the histogram of surface heights at a mean film thickness of $\bar{h}$ = 1200 nm together with the probability-density curve of a gamma distribution whose shape a and scale b parameters were estimated from $\bar{h}$ and σ by the method of moments. In every case the fitted gamma

© 2026 by the author(s). Distributed under a Creative Commons CC BY license.

Preprints.org (www.preprints.org) | NOT PEER-REVIEWED | Posted: 4 March 2026 doi:10.20944/preprints202603.0309.v1

curve reproduces the measured histogram well. To assess goodness of fit as $\bar{h}$ varies, the gamma and normal models were compared using the Kullback–Leibler divergence D_{KL}, defined for an observed distribution $P = \{p_j\}$ and a model $Q = \{q_j\}$ as

$$D_{\mathrm{KL}}(P||Q) = \sum_j p_j \log \frac{p_j}{q_j} \tag{26}$$

with smaller values indicating better agreement [35]. Figure 9 plots D_{KL} versus $\bar{h}$: the solid line corresponds to the gamma-distribution model, while the dashed line represents the normal distribution model. Since the rate parameter of a normal distribution is independent of $\bar{h}$, its D_{KL} remains constant. In contrast, the gamma model provides a markedly better fit. Because the polished ball surfaces used in this study exhibit negative skewness, the corresponding oil film thickness distribution, which is the inverted surface profile, has positive skewness. A gamma distribution inherently possesses positive skewness, quantified as $2/\sqrt{a}$, whereas a normal distribution is symmetric with zero skewness; this asymmetry enables the gamma model to match the experimental data more accurately than the normal model. When $\bar{h}/\sigma$ approached 1, the D_{KL} obtained with the gamma fit increased. At this point, as indicated by Eq.15, the shape parameter a also approaches 1. As a result, the gamma probability density function progressively develops a long right tail and, at a = 1, converges to the exponential distribution. This theoretical tendency supports the observation in Figure 5 that $\bar{h}_{\mathrm{rough}}$ approaches σ in the low-speed regime. However, the actual measured distribution deviates from the exponential distribution, and the gamma distribution can no longer adequately reproduce it, causing D_{KL} to become large. A rigorous description of the thickness distribution under contact conditions therefore remains an outstanding topic for future work.

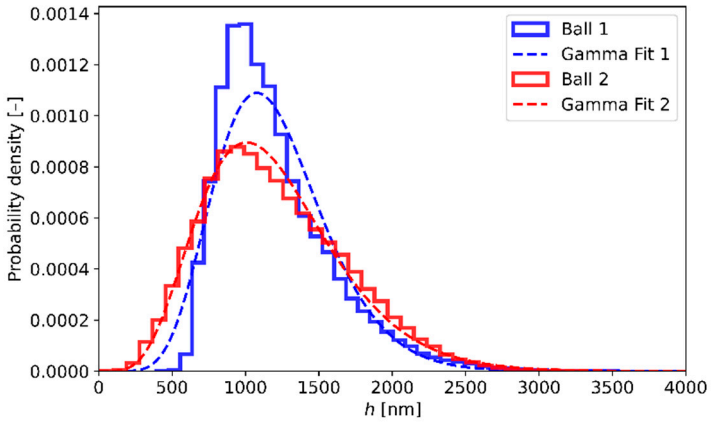

Figure 8. Gamma distribution fit to the estimated oil film thickness distribution H at $\bar{h}$ = 1200 nm. The step histogram represents H obtained by inverting the measured surface profile and applying the $\bar{h}$ offset. The dashed curve is the gamma probability density derived by the method of moments using $\bar{h}$ and σ. Blue lines correspond to Ball 1, and red to Ball 2.

© 2026 by the author(s). Distributed under a Creative Commons CC BY license.

Preprints.org (www.preprints.org) | NOT PEER-REVIEWED | Posted: 4 March 2026 doi:10.20944/preprints202603.0309.v1

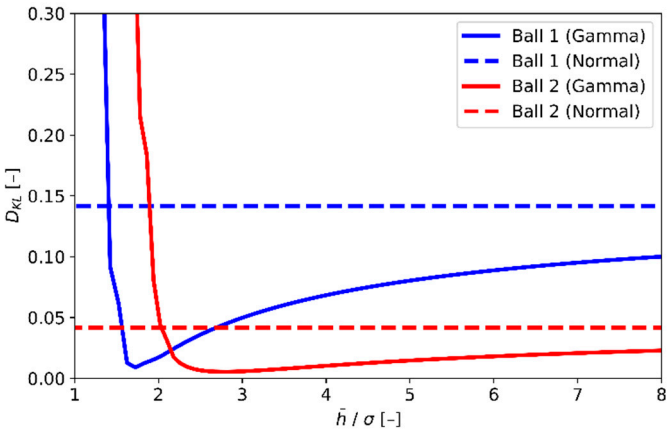

Figure 9. Kullback–Leibler divergence D_{KL} of the oil film thickness distribution H for various $\bar{h}/\sigma$ values, evaluated under two parametric assumptions. The solid curve shows the divergence when H is modeled by a gamma distribution fitted via the method of moments, whereas the dashed curve corresponds to a normal distribution fitted to the same data.

Figure 10 shows the $\mathbb{E}[1/H] \times \mathbb{E}[H]$ for Ball 1, Ball 2, and the gamma distribution. This value is theoretically equal to the capacitance ratio C/C_{flat} shown in Figure 7. The results show closer agreement with Ball 2 than with Ball 1, suggesting that the distribution of the gap formed between the two surfaces of Ball 2 is better represented by a gamma distribution. Nevertheless, in both cases the deviation from the gamma approximation remains small, indicating that the gamma distribution provides a reasonable approximation for the capacitance increase due to surface roughness. Therefore, the analytically accessible value of $\mathbb{E}[1/H]$ derived from the gamma approximation can be considered adequate for subsequent analysis of the parallel-plate model. It should be noted that an alternative method for computing $\mathbb{E}[1/H]$ applicable to a wider range of non-normal distributions is presented in Appendix B.

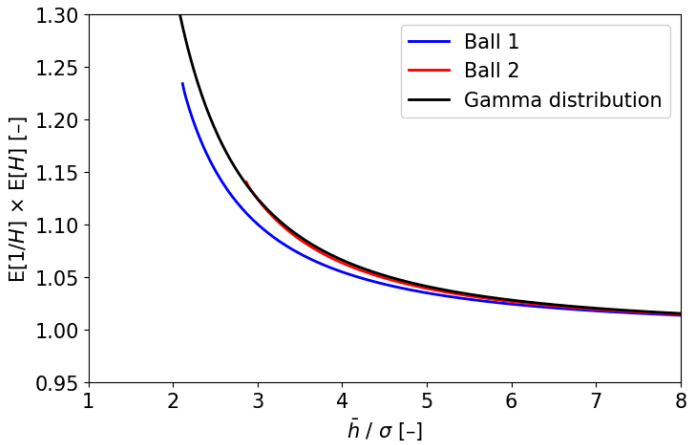

Figure 10. Relationship between $\mathbb{E}[1/H] \times \mathbb{E}[H]$ and $\bar{h}/\sigma$. The blue solid line represents Ball 1, the red solid line Ball 2, and the black solid line the theoretical value when H is modeled by a gamma distribution.

5.3. Inverse Determination of Surface Roughness from Film Thickness Measurements

Up to this point the surface roughness σ has been regarded as known, and the focus has been on correcting the impedance-derived film thickness $h_{1,flat}$. In contrast, the problem can be inverted. If $h_{1,flat}$ is forced to agree with a reference film thickness obtained by an independent method, then the roughness amplitude can be determined in situ. Rearranging Eqs. (21) and (22) to solve for σ explicitly, when the target value is h_{HD}, the solution takes the form,

© 2026 by the author(s). Distributed under a Creative Commons CC BY license.

Preprints.org (www.preprints.org) | NOT PEER-REVIEWED | Posted: 4 March 2026 doi:10.20944/preprints202603.0309.v1

$$\sigma = \frac{h_{1,\mathrm{flat}}}{2}\sqrt{\left(\frac{2h_{\mathrm{HD}}}{(1-\alpha)h_{1,\mathrm{flat}}} - 1\right)^2 - 1} \tag{27}$$

Figure 11 plots the roughness estimates extracted from ball-on-disc experiments together with the surface roughness measured directly using an optical interference microscope. For entrainment speeds $v \geq 0.15$ m/s the estimates coincide with the measurements, demonstrating high sensitivity of the method. Above $v \approx 0.30$ m/s, the scatter increases because the difference between $h_{1,\mathrm{flat}}$ and h_{HD} becomes small at high speed, even a slight correction to $h_{1,\mathrm{flat}}$ strongly influences the computed σ. The estimated roughness decreases as v is lowered. This speed range corresponds to the regime in which the shape parameter a approaches 1, and the reduction is attributed to the mismatch that arises when the gap-height distribution is assumed to follow a gamma distribution. It should be noted that for Ball 0, whose surface roughness measured by white-light interferometry was negligibly small, the inverse analysis overestimated the roughness amplitude. This overestimation is attributed to the macroscopic film thickness variation inherent in EHD contacts, which the present model interprets as surface roughness. A detailed discussion of this effect is given in Appendix C.

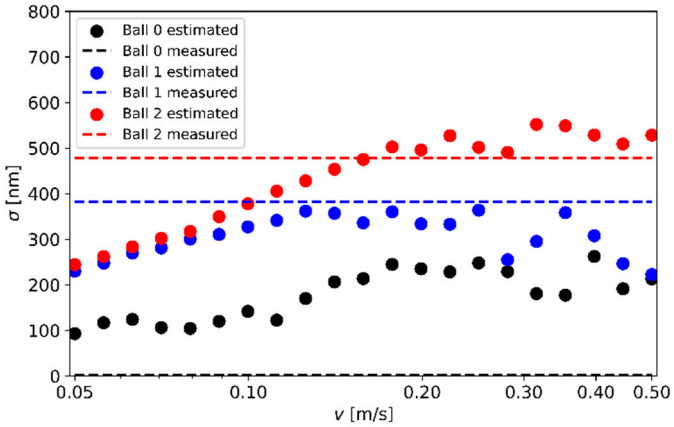

Figure 11. Variation of the σ obtained by adjusting the EIM-based reference film thickness $h_{1,\mathrm{flat}}$ so that it matches the Hamrock-Dowson equation h_{HD} at each entrainment speed. Lubricant: PAO (kinematic viscosity at 40 °C: 426.6 mm²/s; normal load: F_N = 22.4 N; slide-to-roll ratio: 0 (pure rolling). Filled circles represent the σ values estimated by EIM and h_{HD}, whereas dashed lines correspond to the experimentally measured σ by optical interference microscope. Black, blue, and red symbols/lines correspond to Ball 0, Ball 1, and Ball 2, respectively.

6. Conclusions

In this study, the metallic contact region and the lubricating oil film region were represented by an RC parallel circuit, and the oil film thickness was modeled as a random variable H whose spatial distribution reflects the surface roughness profile. This modeling approach allowed us to construct a theoretical framework for an EIM that incorporates surface roughness. We showed that the capacitance increases in proportion to $\mathbb{E}[1/H]$ and, since $1/H$ is a convex function of H, Jensen's inequality directly explains why any roughness-based model necessarily predicts a larger capacitance than the ideal parallel-plate model. Because the gamma distribution is strictly positive and its expectation of the reciprocal admits a closed-form expression, we adopted it as the statistical model for film thickness. Using parameters obtained via the method of moments, we derived a correction formula that converts the conventional EIM mean film thickness $h_{1,\mathrm{flat}}$ into a roughness-compensated value. When this formula was applied to ball-on-disc experiments, the film thickness that had been underestimated for rough specimens was brought into better agreement with both the Hamrock-Dowson equation and interferometric measurements, indicating that the proposed method can correct oil film thickness estimates. However, in the thin-film regime where the ratio $\bar{h}/\sigma$ approaches

© 2026 by the author(s). Distributed under a Creative Commons CC BY license.

Preprints.org (www.preprints.org) | NOT PEER-REVIEWED | Posted: 4 March 2026 doi:10.20944/preprints202603.0309.v1

unity, the gamma distribution degenerates toward an exponential distribution, so it no longer reflects the actual distribution, and the accuracy degrades.

Author Contributions: Conceptualization, F.A. and T.M.; methodology, D.K. and F.A.; software, D.K. and F.A.; validation, D.K. and F.A.; formal analysis, D.K.; investigation, D.K.; resources, D.K. and S.I.; data curation, D.K., S.I., and F.A.; writing—original draft preparation, D.K.; writing—review and editing, F.A., S.I., T.M. and S.M.; visualization, D.K.; supervision, T.M. and S.M.; project administration, T.M. and S.M.; and funding acquisition, T.M. and S.M. All authors have read and agreed to the published version of the manuscript.

Funding: This research received no external funding.

Data Availability Statement: Data is contained within the article.

Acknowledgments: The test specimens used in this study were prepared by Takahito Shimada of NSK Ltd. In writing this paper, we received much advice through discussions conducted with Kosei Yamaguchi, Keisuke Manabe, Yasuo Matsuzaki, and Kazunori Nakagawa, of NSK Ltd. Furthermore, Keisuke Yokoyama and Kenichi Shibasaki of NSK Ltd. provided much support for this work. We would like to express our gratitude to these people.

Conflicts of Interest: The authors declare no conflict of interest.

Nomenclature

a	Gamma distribution shape parameter	[–]
b	Gamma distribution rate parameter	[–]
c	Hertzian contact radius	[m]
h	Oil film thickness	[m]
$\bar{h}$	Mean oil-film thickness in the contact area	[m]
$\bar{h}_{\mathrm{flat}}$	Mean oil film thickness in the contact area obtained by the conventional method	[m]
$\bar{h}_{\mathrm{rough}}$	Mean oil film thickness in the contact area obtained by the proposed method	[m]
h_1	Mean oil film thickness within the contact area that behaves as a capacitor	[m]
$h_{1,\mathrm{flat}}$	Mean oil film thickness within the contact area that behaves as a capacitor obtained by the conventional method	[m]
$h_{1,\mathrm{rough}}$	Mean oil film thickness within the contact area that behaves as a capacitor obtained by the proposed method	[m]
$h_{\mathrm{H\text{-}D}}$	Central oil film thickness calculated by the Hamrock-Dowson equation	[m]
h_{min}	Minimum oil film thickness within the contact area	[m]
h_{max}	Maximum oil film thickness within the contact area	[m]
n	Length of the array	[–]
p	Realizations of the observed distribution	[–]
q	Realizations of the predicted distribution	[–]
r_b	Ball radius	[m]
u	Electrostatic energy density	[J/m^3]
v	Entrainment speed	[m/s]
C	Capacitance	[F]
C_1	Capacitance in lubricated area within the contact area	[F]
C_2	Capacitance in surrounding area	[F]
D_{KL}	Kullback–Leibler divergence	[–]
F_N	Normal force	[N]
P	Observed distribution	[–]
Q	Predicted distribution	[–]
R_t	Track radius	[m]

© 2026 by the author(s). Distributed under a Creative Commons CC BY license.

Preprints.org (www.preprints.org) | NOT PEER-REVIEWED | Posted: 4 March 2026 doi:10.20944/preprints202603.0309.v1

S	Area of the Hertzian contact region	[m²]
E	Electric field	[V/m]
$\mathbb{E}[\cdot]$	Expectation operator	
H	Random variable of oil film thickness on a rough surface	[m]
M	Torque	[Nm]
U	Electrostatic energy	[J]
V	Voltage	[V]
Z	Complex impedance	[Ω]
$\lvert Z \rvert$	Magnitude of complex impedance	[Ω]
α	Oil film breakdown ratio	[–]
γ_1	Skewness of surface roughness	[–]
γ_2	Kurtosis of the surface roughness	[–]
$\Gamma(\cdot)$	Gamma function	
ε_0	Permittivity of vacuum	[F/m]
ε_r	Relative permittivity of oil	[–]
ε	Permittivity of oil	[F/m]
θ	Phase angle of impedance	[rad]
σ	Standard deviation of surface roughness	[m]
ω	Angular frequencies of the applied voltage	[rad/s]
$\mathfrak{W}(\cdot)$	Lambert W function	

Abbreviations

The following abbreviations are used in this manuscript:

EHD	Elastohydrodynamic
EIM	Electrical impedance method
ITO	Indium tin oxide

Appendix A Analysis of the Wavenumber-Dependent Effect of Surface Roughness on Capacitance

In the main text we attributed the discrepancy between the capacitances obtained with the parallel-plate pixel approximation in Figure 7 and those calculated by finite-element electric-field analysis to the neglect of high-wavenumber components. This section tests that explanation through additional simulations. Isotropic random rough surfaces with root-mean-square heights σ of 100 nm, 200 nm, and 300 nm were numerically generated while varying only their spectral characteristics. The simulated area measured 0.1 mm × 0.1 mm. The one-dimensional mean power spectrum was defined by a roll-off wavenumber q_0, above which the power spectral density decays as a power law, and a cut-off wavenumber q_1, which sets the upper bound of the spectrum and corresponds to the shortest wavelength present on the surface. Six logarithmically spaced values of q_0 ranging from 0.188 to 1.634 μm^{-1} were employed with a fixed q_1 of 1.944 μm^{-1} and a Hurst exponent H of 0.8. By increasing q_0 while keeping q_1 and σ constant, higher-wavenumber components come to dominate the spectrum. Each height map contained 512 × 512 pixels, and the electric field was solved with finite-element analysis. Figure A1 displays two-dimensional color maps of the generated roughness at σ = 200 nm, whereas Fig. A2 and A3 presents the corresponding height histograms and power spectral density curves. These results confirm that the target spectral distributions were accurately reproduced, and that the spectrum can be modified independently without altering the overall statistical form of the surface.

© 2026 by the author(s). Distributed under a Creative Commons CC BY license.

Preprints.org (www.preprints.org) | NOT PEER-REVIEWED | Posted: 4 March 2026 doi:10.20944/preprints202603.0309.v1

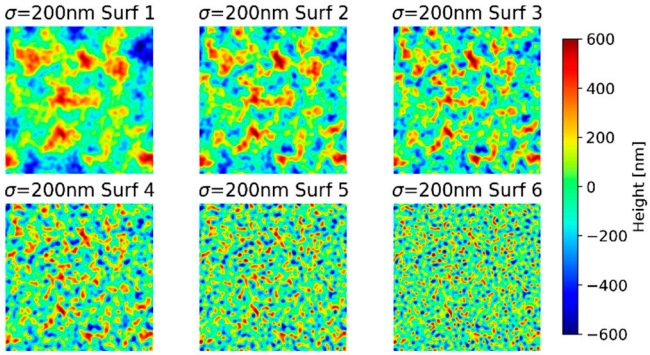

Figure A1. 2d color map of the generated surface height.

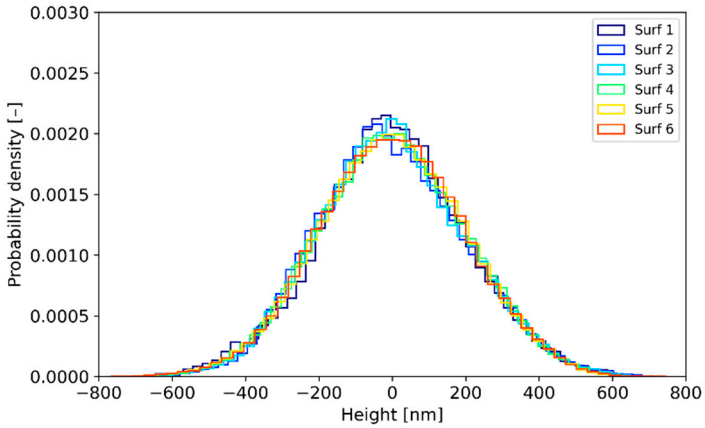

Figure A2. Histogram of height distribution of the generated surface.

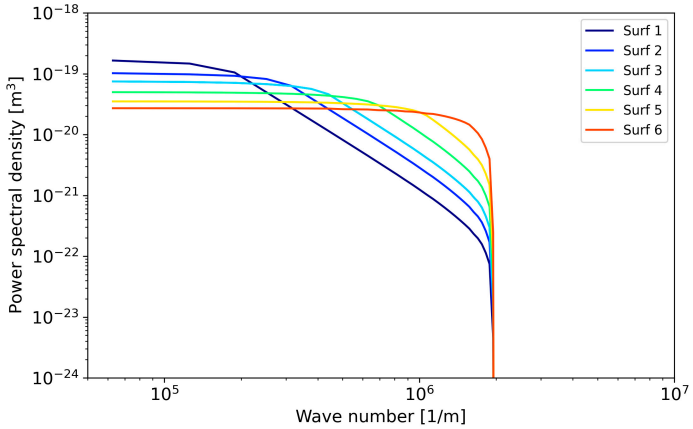

Figure A3. One-dimensional power spectral density of the generated surface (directionally averaged).

For each numerically generated surface, an average film thickness $\bar{h}$ was imposed such that the ratio $\bar{h}/\sigma$ fell between 5 and 10, after which the electrostatic field was solved. Figure A4 presents the resulting capacitance ratio C/C_{flat} referenced to the parallel-plate model: the first axis plots $\bar{h}/\sigma$, the second the common logarithm of q_0, and the third the calculated capacitance C. The black surface indicates the values obtained from the parallel-plate approximation. Even when topographies share an identical height distribution, the capacitance increases as q_0 becomes larger—that is, as the amplitude of the high-frequency spectral components grows. When q_0 is small, the ratio converges

© 2026 by the author(s). Distributed under a Creative Commons CC BY license.

Preprints.org (www.preprints.org) | NOT PEER-REVIEWED | Posted: 4 March 2026 doi:10.20944/preprints202603.0309.v1

asymptotically toward the parallel-plate prediction, confirming that high-wavenumber content drives the excess capacitance. The increase is also more pronounced for larger σ. These trends provide a consistent physical explanation for the divergence previously observed between the finite-element results and the parallel-plate approximation. Developing a rigorous mathematical framework that quantitatively captures this behavior is left to future work.

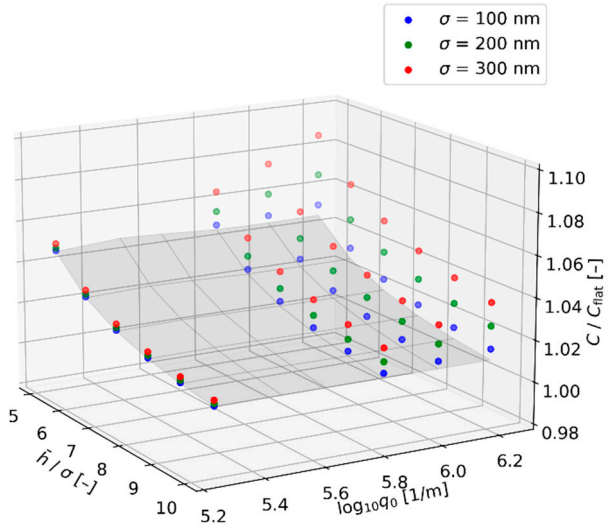

Figure A4. Three-dimensional map of the capacitance ratio C/C_{flat} obtained from finite-element field analysis (colored scatter). The first axis gives the $\bar{h}/\sigma$; the second axis shows the common logarithm of the roll off wave number q_0; the third axis gives the calculated capacitance C. The black mesh represents the values predicted by the parallel-plate approximation for the same surfaces. Results are shown for three roughness levels, σ = 100 nm, 200 nm, and 300 nm.

Appendix B Approximation of $\mathbb{E}[1/H]$ Using a Taylor Expansion

In this study, a gamma-distribution-based approach was adopted owing to its advantage of yielding a closed-form expression for the roughness statistic $\mathbb{E}[1/H]$. However, the gamma distribution has an inherent limitation in that its skewness and kurtosis are uniquely determined by the shape parameters a and b, which restricts its ability to represent surface roughness distributions exhibiting a wide range of non-normal distributions. To address this limitation, an alternative approach based on a Taylor expansion was also investigated for deriving $\mathbb{E}[1/H]$.

Expanding the function f(h) = 1/h about the mean $\bar{h} = \mathbb{E}[H]$ up to fourth order gives

$$f(H) = f(\bar{h}) + f'(\bar{h})(H-\bar{h}) + \frac{f''(\bar{h})}{2}(H-\bar{h})^2 + \frac{f'''(\bar{h})}{6}(H-\bar{h})^3 + \frac{f''''(\bar{h})}{24}(H-\bar{h})^4 \quad \text{(B1)}$$

$$\frac{1}{H} = \frac{1}{\bar{h}} - \frac{(H-\bar{h})}{\bar{h}^2} + \frac{(H-\bar{h})^2}{\bar{h}^3} - \frac{(H-\bar{h})^3}{\bar{h}^4} + \frac{(H-\bar{h})^4}{\bar{h}^5} \quad \text{(B2)}$$

Taking the expectation of both sides and noting that $\mathbb{E}[H-\bar{h}] = 0$, one obtains

$$\mathbb{E}\left[\frac{1}{H}\right] = \frac{1}{\bar{h}} + \frac{\mathbb{E}[(H-\bar{h})^2]}{\bar{h}^3} - \frac{\mathbb{E}[(H-\bar{h})^3]}{\bar{h}^4} + \frac{\mathbb{E}[(H-\bar{h})^4]}{\bar{h}^5} \quad \text{(B3)}$$

Substituting the definitions of the variance σ^2, skewness γ_1, and kurtosis γ_2 and rearranging yields

© 2026 by the author(s). Distributed under a Creative Commons CC BY license.

Preprints.org (www.preprints.org) | NOT PEER-REVIEWED | Posted: 4 March 2026 doi:10.20944/preprints202603.0309.v1

$$\sigma^2 = \mathbb{E}[(H - \bar{h})^2] \tag{B4}$$

$$\gamma_1 = \frac{\mathbb{E}[(H - \bar{h})^3]}{\sigma^3} \tag{B5}$$

$$\gamma_2 = \frac{\mathbb{E}[(H - \bar{h})^4]}{\sigma^4} \tag{B6}$$

$$\mathbb{E}\left[\frac{1}{H}\right] = \frac{1}{\bar{h}}\left(1 + \frac{\sigma^2}{\bar{h}^2} - \gamma_1\frac{\sigma^3}{\bar{h}^3} + \gamma_2\frac{\sigma^4}{\bar{h}^4}\right) \tag{B7}$$

Since this expression incorporates skewness and kurtosis in addition to the mean and variance, it enables evaluation of $\mathbb{E}[1/H]$ in a distribution-free manner that accounts for non-normal distributions. Substituting into Equation (11), $\mathbb{E}[1/H]$ can be expressed in terms of $h_{1,\mathrm{flat}}$ and $h_{1,\mathrm{rough}}$ as follows

$$h_{1,\mathrm{rough}}{}^5 - h_{1,\mathrm{flat}}h_{1,\mathrm{rough}}{}^4 - \sigma^2 h_{1,\mathrm{flat}}h_{1,\mathrm{rough}}{}^2 + \sigma^3\gamma_1 h_{1,\mathrm{flat}}h_{1,\mathrm{rough}} - \sigma^4\gamma_2 h_{1,\mathrm{flat}} = 0 \tag{B8}$$

Since this equation does not admit a closed-form solution and must be solved numerically, the gamma distribution approximation, which yields an analytically tractable expression for $\mathbb{E}[1/H]$, was adopted as the primary method in this study.

Appendix C Effect of macroscopic EHD film geometry on roughness estimation

Although the surface roughness of Ball 0, determined by white-light interferometry, was negligibly small, the inverse analysis produced a roughness amplitude that exceeded the measured surface roughness by a significant margin. Under conditions of high viscosity and low surface roughness, the pronounced horseshoe-shaped film thickness profile characteristic of EHD contacts emerges, resulting in a spatially non-uniform film thickness distribution across the contact area. Since the present model interprets this spatial variation in film thickness as surface roughness, the inverse analysis yields an overestimated roughness amplitude.

Figure A5 provides a color image of the EHD contact area, whereas Fig. C2 plots the film thickness profiles measured along the contact centerline at each v. Because the present formulation does not account for this macroscopic film geometry, a discrepancy arises. Ideally, the height variation associated with the macroscopic film shape should be superimposed on the microscopic surface roughness. Such a distribution cannot be represented by a gamma distribution and must instead be obtained through numerical analysis. The results indicate that, once $h_{1,\mathrm{flat}}$ is corrected appropriately, in-situ monitoring of the complete film thickness distribution, including its global shape, should be feasible.

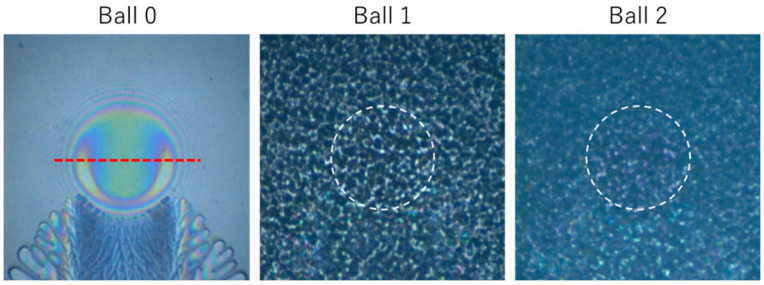

Figure A5. Colored image of the EHD contact area acquired at an entrainment speed of v = 0.126 m/s. The red line marks the track along which the film thickness was measured, and the white circles outline the estimated contact regions for Ball 1 and Ball 2.

© 2026 by the author(s). Distributed under a Creative Commons CC BY license.

Preprints.org (www.preprints.org) | NOT PEER-REVIEWED | Posted: 4 March 2026 doi:10.20944/preprints202603.0309.v1

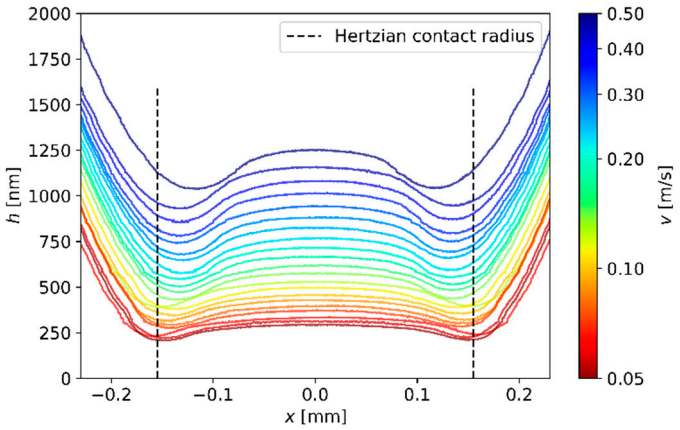

Figure A6. Cross-sections of h profiles for Ball 0, measured by optical interferometry at each entrainment speed v. Each colored line corresponds to the speed indicated on the accompanying color bar, while the dashed lines indicate the radius of the contact circle under normal load of F_N = 22.4 N.

References

1. Dowson, D.; Higginson, G.R. A numerical solution to the elasto-hydrodynamic problem. *J. Mech. Eng. Sci.* **1959**, *1*, 6–14.
2. Hamrock, B.J.; Dowson, D. Isothermal elastohydrodynamic lubrication of point contacts. Part III—Fully flooded results. *ASME J. Lubr. Technol.* **1977**, *99*, 264–275.
3. Dyer, D.; Stewart, R.M. Detection of rolling element bearing damage by statistical vibration analysis. *J. Mech. Des.* **1978**, *100*, 229–235.
4. Kiral, Z.; Karagülle, H. Simulation and analysis of vibration signals generated by rolling element bearing with defects. *Tribol. Int.* **2003**, *36*, 667–678.
5. Saruhan, H.; Sarıdemir, S.; Çiçek, A.; Uygur, Ö. Vibration Analysis of Rolling Element Bearings Defects. *J. Appl. Res. Technol.* **2014**, *12*, 384–395.
6. Cambow, R.; Singh, M.; Bagha, A.K.; Singh, H. To compare the effect of different level of self-lubrication for bearings using statistical analysis of vibration signal. *Mater. Today Proc.* **2018**, *5*, 28364–28373.
7. Mba, D. Acoustic emissions and monitoring bearing health. *Tribol. Trans.* **2003**, *46*, 447–451.
8. Johnston, G.J.; Wayte, R.; Spikes, H.A. The Measurement and Study of Very Thin Lubricant Films in Concentrated Contacts. *Tribol. Trans.* **1991**, *34*, 187–194.
9. Kaneta, M.; Sakai, T.; Nishikawa, H. Effects of Surface Roughness on Point Contact EHL. *Tribol. Trans.* **1993**, *36*, 605–612.
10. Sugimura, J.; Jones, W.R. Jr.; Spikes, H.A. EHD film thickness in non-steady state contacts. *J. Tribol.* **1998**, *120*, 442–449.
11. Guegan, J.; Kadiric, A.; Gabelli, A.; Spikes, H. The relationship between friction and film thickness in EHD point contacts in the presence of longitudinal roughness. *Tribol. Lett.* **2016**, *64*, 33.
12. Czichos, H. Influence of asperity contact conditions on the failure of sliding elastohydrodynamic contacts. *Wear* **1977**, *41*, 1–14.
13. Lugt, P.M.; Severt, R.W.M.; Fogelström, J.; Tripp, J.H. Influence of surface topography on friction, film breakdown and running-in in the mixed lubrication regime. *Proc. Inst. Mech. Eng., Part J* **2001**, *215*, 519–533.
14. Lord, J.; Larsson, R. Film-forming capability in rough surface EHL investigated using contact resistance. *Tribol. Int.* **2008**, *41*, 831–838.
15. Jablonka, K.; Glovnea, R.; Bongaerts, J. Evaluation of EHD films by electrical capacitance. *J. Phys. D-Appl. Phys.* **2012**, **45**, 385301.
16. Jablonka, K.; Glovnea, R.; Bongaerts, J.; Morales-Espejel, G. The effect of lubricant polarity upon capacitance measurements of EHD contacts. *Tribol. Int.* **2013**, **61**, 95–101.
17. Gonda, A.; Paulus, S.; Graf, S.; Koch, O.; Götz, S.; Sauer, B. Basic experimental and numerical investigations to improve the modeling of the electrical capacitance of rolling bearings. *Tribol. Int.* **2024**, *193*, 109354.

© 2026 by the author(s). Distributed under a Creative Commons CC BY license.

Preprints.org (www.preprints.org) | NOT PEER-REVIEWED | Posted: 4 March 2026 doi:10.20944/preprints202603.0309.v1

18. Maruyama, T.; Nakano, K. In Situ Quantification of Oil Film Formation and Breakdown in EHD Contacts. *Tribol. Trans.* **2018**, *61*, 1057–1066.
19. Maruyama, T.; Maeda, M.; Nakano, K. Lubrication Condition Monitoring of Practical Ball Bearings by Electrical Impedance Method. *Tribol. Online* **2019**, *14*, 327–338.
20. Maruyama, T.; Radzi, F.; Sato, T.; Iwase, S.; Maeda, M.; Nakano, K. Lubrication Condition Monitoring in EHD Line Contacts of Thrust Needle Roller Bearing Using the Electrical Impedance Method. *Lubricants* **2023**, *11*, 223.
21. Iwase, S.; Maruyama, T.; Momozono, S.; Maegawa, S.; Itoigawa, F. Studies on dielectric spectroscopy of oxidatively degraded poly(α-olefin). *Front. Mech. Eng.* **2024**, *10*, 1504347.
22. Maruyama, T.; Kosugi, D.; Iwase, S.; Maeda, M.; Nakano, K.; Momozono, S. Application of the electrical impedance method to steel/steel EHD point contacts. *Front. Mech. Eng.* **2024**, *10*, 1489311.
23. Furtmann, A.; Poll, G. Evaluation of Oil-Film Thickness Along the Path of Contact in a Gear Mesh by Capacitance Measurement. *Tribol. Online* **2016**, *11*, 189–194.
24. Watanabe, A.; Okubo, H.; Nakano, K. In-situ electrical impedance observation for lubrication conditions of gears under actual operation. *Tribol. Int.* **2025**, *210*, 110777.
25. Zhao, Y.-P.; Wang, G.-C.; Lu, T.-M.; Palasantzas, G.; De Hosson, J.Th.M. Surface-roughness effect on capacitance and leakage current of an insulating film. *Phys. Rev. B* **1999**, *60*, 9157–9164.
26. Albina, A.; Taberna, P.L.; Cambronne, J.P.; Simon, P.; Flahaut, E.; Lebey, T. Impact of the surface roughness on the electrical capacitance. *Microelectron. J.* **2006**, *37*, 752–758.
27. Torabi, S.; Cherry, M.; Duijnstee, E.A.; Le Corre, V.M.; Qiu, L.; Hummelen, J.C.; Palasantzas, G.; Koster, L.J.A. Rough Electrode Creates Excess Capacitance in Thin-Film Capacitors. *ACS Appl. Mater. Interfaces* **2017**, *9*, 27290–27297.
28. Greenwood, J.A.; Williamson, J.B.P. Contact of nominally flat surfaces. *Proc. R. Soc. A* **1966**, *295*, 300–319.
29. Nayak, P.R. Random Process Model of Rough Surfaces. *J. Lubr. Technol.* **1971**, *93*, 398–407.
30. Patir, N.; Cheng, H.S. An Average Flow Model for Determining Effects of Three-Dimensional Roughness on Partial Hydrodynamic Lubrication. *J. Lubr. Technol.* **1978**, *100*, 12–17.
31. Morris, S.A.; Leighton, M.; Morris, N.J. Electrical Field Strength in Rough Infinite Line Contact Elastohydrodynamic Conjunctions. *Lubricants* **2022**, *10*, 87.
32. Sunahara, K.; Yamashita, S.; Yamamoto, M.; Ikeda, M.; Nishikawa, H.; Matsuda, K.; Kaneta, M. Development of Grease Film Breakdown Observing Device. *Tribol. Online* **2008**, *3*, 40–43.
33. Kant, R.; Goel, H. In Situ Electrochemical Impedance Spectroscopic Method for Determination of Surface Roughness and Morphological Convexity. *J. Phys. Chem. Lett.* **2021**, *12*, 10025–10033.
34. Jensen, J.L.W.V. Sur les fonctions convexes et les inégalités entre les valeurs moyennes. *Acta Math.* **1906**, *30*, 175–193.
35. Kullback, S.; Leibler, R.A. On Information and Sufficiency. *Ann. Math. Stat.* **1951**, *22*, 79–86.

Disclaimer/Publisher's Note: The statements, opinions and data contained in all publications are solely those of the individual author(s) and contributor(s) and not of MDPI and/or the editor(s). MDPI and/or the editor(s) disclaim responsibility for any injury to people or property resulting from any ideas, methods, instructions or products referred to in the content.

© 2026 by the author(s). Distributed under a Creative Commons CC BY license.